Biocybernetics and Biomedical Engineering 45 (2025) 438–450

Contents lists available at ScienceDirect

Biocybernetics and Biomedical Engineering

journal homepage: www.elsevier.com/locate/bbe

Integrative and interpretable framework to unveil the neurophysiological fingerprint of Alzheimer's disease and mild cognitive impairment: A machine learning-SHAP approach

Víctor Gutiérrez-de Pablo[a,b,*], María Herrero-Tudela[a,b], Marina Sandonís-Fernández[a], Jesús Poza[a,b,c], Aarón Maturana-Candelas[a,b], Víctor Rodríguez-González[a,b], Miguel Ángel Tola-Arribas[b,d], Mónica Cano[e], Hideyuki Hoshi[f], Yoshihito Shigihara[f], Roberto Hornero[a,b,c], Carlos Gómez[a,b]

[a] Biomedical Engineering Group, University of Valladolid, Valladolid, Spain
[b] Centro de Investigación Biomédica en Red de Bioingeniería, Biomateriales y Nanomedicina (CIBER-BBN), Madrid, Spain
[c] IMUVA, Instituto de Investigación en Matemáticas, University of Valladolid, Valladolid, Spain
[d] Department of Neurology, Hospital Universitario Rio Hortega, Valladolid, Spain
[e] Department of Clinical Neurophysiology, Hospital Universitario Rio Hortega, Valladolid, Spain
[f] Precision Medicine Centre, Hokuto Hospital, Obihiro, Japan

ARTICLE INFO

Keywords:
Alzheimer's disease
Mild cognitive impairment
Machine learning
SHAP
Magnetoencephalography
Electroencephalography
Neurophysiological fingerprint

ABSTRACT

Dementia and mild cognitive impairment (MCI) due to Alzheimer's disease (AD) are neurological pathologies associated with disruptions in brain electromagnetic activity, typically studied using magnetoencephalography (MEG) and electroencephalography (EEG). To quantify diverse brain properties, different families of parameters can be computed from MEG and EEG (i.e., spectral, non-linear, morphological, functional connectivity, or network structure and organisation). However, studying these characteristics separately overlooks the complex nature of brain activity. Integrative frameworks can be useful to unveil the intricate neurophysiological fingerprint, as well as to characterise pathological conditions comprehensively. To that purpose, data fusion methodologies are crucial, despite their interpretational challenges. In this study, Machine Learning (ML) models were trained to discriminate between groups of severity, whereas the SHapley Additive eXplanations (SHAP) algorithm was afterwards utilised to assess the relevance of the input characteristics into the output classification. Three databases were analysed: MEG (55 healthy controls, HC, 42 MCI patients, and 86 AD patients), EEG1 (51 HC, 52 MCI, and 100 AD), and EEG2 (45 HC, 69 MCI, and 82 AD). The best results for the three-class classification problem were obtained by Gradient Boosting for the MEG database: 3-class Cohen's kappa coefficient of 0.5452 and accuracy of 72.63 %. Afterwards, using SHAP on Gradient Boosting, it has been shown that spectral features were identified as highly relevant across all databases. Furthermore, morphology measures presented high relevance for the MEG database, whereas EEG1 and EEG2 databases showed functional connectivity and multiplex organisation measures, respectively, as relevant subgroups of parameters. Finally, commonly relevant features across databases were selected using SHAP to generate the neurophysiological fingerprints of AD and MCI. This study highlights the relevance of different MEG and EEG parameters in characterising neurological pathologies. The proposed framework, based on MEG and EEG, can be used to generate interpretable, robust, and accurate neurophysiological fingerprints of AD and MCI.

1. Introduction

Alzheimer's disease (AD) is the most common cause of dementia, presenting a significant clinical and social challenge worldwide, particularly in developed countries [1]. AD is characterised by the presence of cognitive, behavioural, memory, and functional dysfunctions, inducing progressive neuronal damage that ultimately results in death [1]. As AD progresses, diverse stages have been identified, from mild to severe symptomatology [1]. Prior to clinical AD, a prodromal condition named mild cognitive impairment (MCI) is likely to occur [2]. MCI is

* Corresponding author at: Biomedical Engineering Group, E.T.S. Ingenieros de Telecomunicación, Universidad de Valladolid, Campus Miguel Delibes, Paseo Belén 15, 47011, Valladolid, Spain.
E-mail address: victor.gutierrez@uva.es (V. Gutiérrez-de Pablo).

https://doi.org/10.1016/j.bbe.2025.05.011
Received 25 July 2024; Received in revised form 21 April 2025; Accepted 31 May 2025
Available online 14 June 2025

defined as an heterogeneous construct of symptoms characterised by small impairments in cognition, function, and memory [2]; these symptoms cannot be considered part of the healthy ageing process, but are not severe enough to match a diagnosis of dementia [1]. The diagnosis procedure was defined in 2018 by the National Institute of Aging and Alzheimer's Association (NIA-AA), designing a scheme for defining and staging the disease across its progression [3]. This framework provides a full depiction of the neurodegeneration that MCI and AD induce in the brain by means of the use of different techniques such as positron emission tomography (PET), functional magnetic resonance imaging (fMRI), and/or the extraction of cerebrospinal fluid (CSF) [3]. However, due to their invasiveness and cost, these methods are not frequently applied [4]. Therefore, alternative or supporting techniques are required to help in AD and MCI diagnosis.

Previous studies have shown that both magnetoencephalography (MEG) and electroencephalography (EEG) can be useful for characterising the brain alterations suffered by AD and MCI patients [4,5]. Both MEG and EEG (M/EEG hereinafter) offer several advantages compared to other techniques, like their high temporal resolution and non-invasiveness [6]. Therefore, neurodegenerative states have been previously characterised by means of different M/EEG measures such as spectral, non-linear, morphological, and based on functional connectivity and network organisation. These metrics have proven useful in assessing brain activity alterations associated with AD and MCI: slowing, loss of complexity and irregularity, and disruption in connectivity and network patterns [7–12]. Due to the complex nature of the brain, their integrated use may provide more robust outcomes. In that sense, in a previous study we introduced a new framework based on association networks (ANs) to generate the map that summarises the organisation of brain activity by means of the analysis of the statistical relationships between M/EEG parameters [13]. However, this methodology provided a limited ability to discriminate between healthy controls (HC) and patients with AD, and its interpretability was limited [13].

In order to provide a better discrimination between groups, diverse machine learning (ML) techniques have been employed in previous literature, including linear discriminant analysis (LDA) [14], quadratic discriminant analysis (QDA) [14], support vector machines (SVM) [15], decision trees [16], and multilayer perceptron (MLP) [14]. However, complex ML approaches cannot provide an interpretable framework for their results, hindering the analysis of the relevance of M/EEG parameters that characterise brain activity properties. To overcome this limitation, eXplainable Artificial Intelligence (XAI) methodologies aim to enhance the transparency and explainability of ML models [17]. This is the case of Shapley Additive exPlanation (SHAP), that was introduced as an XAI algorithm able to assess the relevance of the input features in a given ML model [18]. SHAP was conceived as an algorithm based on game theory, aiming to equally distribute the model's prediction among the input features [18]. As a result, the average contribution of each input feature is computed as the permutation of all the possibilities of including that characteristic into the model [18]. Thus, the combination of ML and SHAP can provide the relevance of the input metrics into the model, minimising the "black box" problem, inherent in complex ML techniques [19].

To the best of our knowledge, this is the first time an ML-SHAP framework is employed to identify a robust, accurate, and interpretable representation of MCI and dementia due to AD through M/EEG features. This representation, henceforth called neurophysiological fingerprint, enables the assessment of how patients with AD and MCI diverge from the healthy cognition state (i.e., HC) in terms of the most relevant features of the brain functional organisation. Of note, the evaluation of M/EEG parameters to provide a multi-class classification and an interpretation to their relevance is still an open challenge, as the complexity of the classification increases as more classes are included [20].

Hence, we hypothesise that the application of an ML-SHAP-based framework to a comprehensive set of M/EEG parameters is capable of generating the global neurophysiological fingerprints of AD and MCI. To that purpose, the first objective of the study is to extract different M/EEG parameters and use them as input to evaluate different ML models. These will be able to perform a discrimination between groups. Afterwards, the second objective of this study consists in employing the SHAP algorithm to evaluate the relevance of the input characteristics in order to generate the neurophysiological fingerprints of AD and MCI based on the most relevant features. Finally, the third objective is to evaluate the replicability of the methodology; for that purpose, one MEG database and two EEG datasets were used to prove that the proposed framework provides generalisable results.

2. Materials

2.1. Subjects

In this study, three databases were analysed: one MEG database and two EEG databases. The sociodemographic and clinical data of the subjects from the three datasets are displayed in Table 1. The MEG database, acquired at the Hokuto Hospital (Obihiro, Japan) and the Kumagaya General Hospital (Kumagaya, Japan), included 183 participants, divided into 55 HC individuals, 42 patients with MCI, and 86 patients with AD. The first EEG database, referred to as EEG1, encompassed residents of North Portugal and the autonomous region of Castile and Leon (Spain), and comprised 202 participants; these subjects consisted of 51 HC individuals, 51 patients with MCI, and 100 patients with AD. The second EEG database, named EEG2, was acquired at the Department of Clinical Neurophysiology of the Hospital Universitario Río Hortega (Valladolid, Spain) and included 196 participants: 45 HC individuals, 69 patients with MCI, and 82 patients with AD. Patients diagnoses were made in accordance to the standardised criteria of the NIA-AA [21,22]. HC groups consisted of elderly individuals without a history of neurological or psychiatric disorders. Specific inclusion criteria for patients with MCI or AD encompassed a minimum age of 65, and exclusion criteria: neoplasia, other neurological or psychiatric diseases, advanced dementia, recent surgery, hypercatabolic states, vascular pathology, and medications with potential effects on M/EEG activity. To prevent misleading results, the impact of age and sex as confounding factors was evaluated in the parameters under study. Results showed no significant impact of these variables in any of the parameters under analysis (p-value $>$ 0.05, Spearman's correlation coefficient, FDR corrected). For the three databases, resting-state recordings were acquired due to the advanced

Table 1
Socio-demographic and clinical data for each database. AD: Alzheimer's disease; MCI: Mild cognitive impairment; HC: Healthy controls; m: Median; IQR: Interquartile range; M: Male; F: Female; MMSE: Mini-Mental State Examination score.

MEG	Group		
	AD	MCI	HC
Participants	86	42	55
Age (years) (m [IQR])	83.0[76.0, 86.0]	78.5[74.0, 82.0]	75.0[69.2, 78.7]
Sex (M:F)	34:52	11:31	26:29
MMSE (m [IQR])	19.0[14.0, 22.0]	26.5[23.0, 28.0]	29.0[28.0, 30.0]
EEG1	Group		
	AD	MCI	HC
Participants	100	51	51
Age (years) (m [IQR])	82.0[76.0, 86.0]	86.0[81.0, 90.0]	79.0[75.0, 85.5]
Sex (M:F)	28:72	15:36	26:25
MMSE (m [IQR])	20.0[13.0, 22.0]	23.0[21.0, 27.7]	29.0[28.0, 30.0]
EEG2	Group		
	AD	MCI	HC
Participants	82	69	45
Age (years) (m [IQR])	81.6[76.3, 83.5]	77.1[72.2, 80.3]	75.6[73.9, 78.6]
Sex (M:F)	34:48	29:40	14:31
MMSE (m [IQR])	21.0[18.0, 24.0]	27.0[26.0, 28.0]	29.0[28.0, 30.0]

age of the patients, as this condition is more comfortable, simpler, and less demanding than task-related paradigms, especially for people suffering from dementia [4].

Participants, legal representatives, family, or caregivers provided their written informed consent before participating in the study, according to the recommendations of the Code of Ethics of the World Medical Association (Declaration of Helsinki). The protocol was approved by three organisations: a) for MEG database by the Ethics Committee of Kumagaya General Hospital in Kumagaya, Japan (approval numbers: #25, #26, #51, and #76), and Hokuto Hospital in Obihiro, Japan (approval numbers: #1001, #1007-R3, #1020, and #1038); b) for EEG1 database by the Ethics Committee of the University of Porto, Portugal (38/CEUP/2018); and c) for EEG2 database by the Ethics Committee of the "Río Hortega" University Hospital in Valladolid, Spain (36/2014/02).

2.2. MEG recordings and pre-processing

The MEG database included recordings of five minutes of resting-state neural activity, divided in five-seconds epochs. Participants were instructed to remain calm and awake with their eyes closed during data acquisition. Head position was scanned employing five coil markers placed on the patient's head during the recording: 40 mm above the nasion point, 10 mm in front of the tragus on each side, and in both pre-auricular points. The recordings were monitored in real time for safety purposes and to prevent drowsiness. The signals were recorded through a 160-channel MEG Vision PQ1160C (Yokogawa Electric, $f_s = 1000$ Hz) at the Hokuto Hospital and a 160-channel RICOH 160-1 (RICOH Co. Ltd, $f_s = 2000$ Hz) at the Kumagaya General Hospital. Both systems are functionally equivalent, consisting in whole-head 160-channel axial gradiometers systems placed in magnetically-isolated rooms. Afterwards, MEG signals were downsampled at 500 Hz to reduce computational cost and bring the sampling rate of this database in line with EEG databases.

A pre-processing stage was carried out in accordance with the following steps [23]: (i) SOurce-estimate-Utilising Noise-Discarding (SOUND) algorithm performance to remove artefacts [24]; (ii) finite impulse response (FIR) Hamming-window band-pass filtering (order 3000) between 1 and 70 Hz to limit noise bandwidth; (iii) FIR Hamming-window band-stop filtering (order 3000) at 50 Hz to remove power-line noise; (iv) artefact rejection through independent component analysis (ICA); and (v) rejection of epochs contaminated with artefacts by visual inspection.

2.3. EEG recordings and pre-processing

Two EEG databases were also considered in this study. EEG1 database was recorded with a 19-channel Nihon Kohden Neurofax JE-921A ($f_s = 500$ Hz), while EEG2 database was acquired using a 19-channel XLTEK® Natus Medical ($f_s = 200$ Hz). In both databases, resting-state signals were recorded. Participants remained relaxed and awake with their eyes closed during the acquisition. The recordings were evaluated in real time for safety and drowsiness. Brain electrical activity was recorded from electrodes F3, F4, F7, F8, Fp1, Fp2, T3, T4, T5, T6, C3, C4, P3, P4, O1, O2, Fz, Cz, and Pz, following the international 10–20 system. During EEG1 database acquisition, common average reference was employed. In the case of EEG2 database, bipolar registration was used, which was afterwards modified to a common average reference. For both databases, five minutes of resting-state EEG activity were recorded, divided in five-seconds epochs.

Subsequently, the EEG recordings underwent a pre-processing stage by means of the following steps [25,26]: (i) mean removal; (ii) FIR Hamming-window band-pass filtering (order 2000) between 1 and 70 Hz to limit noise bandwidth; (iii) FIR Hamming-window band-stop filtering (order 2000) at 50 Hz to remove power-line noise; (iv) artefact rejection by means of ICA; and (v) visual inspection to remove epochs contaminated with artefacts.

2.4. Source localisation

After acquiring and preprocessing the M/EEG recordings, source-level activity was estimated by means of the standardised Low-Resolution Brain Electromagnetic Tomography (sLORETA) algorithm [27]. This stage aimed to establish a common workspace for all three databases analysed in this study. sLORETA allows the computation of 3D linear solutions for the inverse problem, minimising the volume conduction effects that result from the overlapping of non-homogeneous tissue layers with different conductivity properties. In addition, sLORETA constrains solutions assuming maximal correlation between neighbour neural generators, which leads to spatially smoothed outcomes. An identity matrix was employed as noise covariance, since there were no available noise recordings. The implementation of this method is freely available in the Brainstorm toolbox [28].

The source-level neural generators were grouped into 68 regions of interest (ROIs) based on the Desikan–Killiany atlas. Employing a gyrus-based schema, this atlas assigns different brain regions according to their predominant functionalities [29]. The Desikan-Killiany atlas offers a reasonable trade-off between the spatial resolution at source level and the number of acquisition sensors used on each database [23,30–32].

3. Methods

The workflow of the study was organised into three main steps which are described in the following subsections and summarised in Fig. 1. Once M/EEG signals were preprocessed, **i)** M/EEG features were extracted and categorised in two levels of analysis: local activation (spectral, non-linear, and spectro-temporal morphology features), and global synchronisation (functional connectivity, FC, network properties, and multiplex network organisation parameters). Afterwards, **ii)** different ML classification models were applied to discriminate between HC, patients with MCI, and patients with AD. To that purpose, a nested cross-validation approach was followed [33]. Based on the classification performance, the best ML model was selected. In the next step, **iii)** the SHAP algorithm was employed to estimate the relevance of each feature on the best ML model; moreover, a 10-fold cross-validation strategy, was applied to strengthen our model reliability [34,35]. From SHAP explanation, **iv)** the most relevant features were selected to display the global neurophysiological fingerprints of AD and MCI. Statistically significant differences between groups were calculated for all selected features and databases.

3.1. Feature extraction

In order to characterise the brain activity, multiple M/EEG-derived parameters were considered. A total of 89 features were extracted from the M/EEG signals (see Supplementary Material). These can be categorised in two different levels according to the literature: local activation and global synchronisation [4,36].

The local activation level reflects the properties of specific brain regions [7]. At this level, three subgroups of metrics can be considered:

a) **Spectral parameters**. The metrics included in this subgroup are able to quantify intrinsic features of the spectral content of the signals. They were computed from the normalised power spectral density. The slowing and the alterations in the distribution of neural oscillators that have been observed in neurodegenerative states can be measured by means of relative power (RP), median frequency (MF), individual alpha frequency (IAF), transition frequency (TF), and 95 % spectral edge frequency (SEF95) [14,37,38]. Furthermore, changes in irregularity and diversity of spectral content of the normalised power spectral density have been also observed in neurodegenerative diseases; they can be quantified using metrics such as spectral entropy (SE), Tsallis entropy (TsE), Escort-Tsallis entropy (ETsE), and Rènyi entropy (RE) [8,38,39].

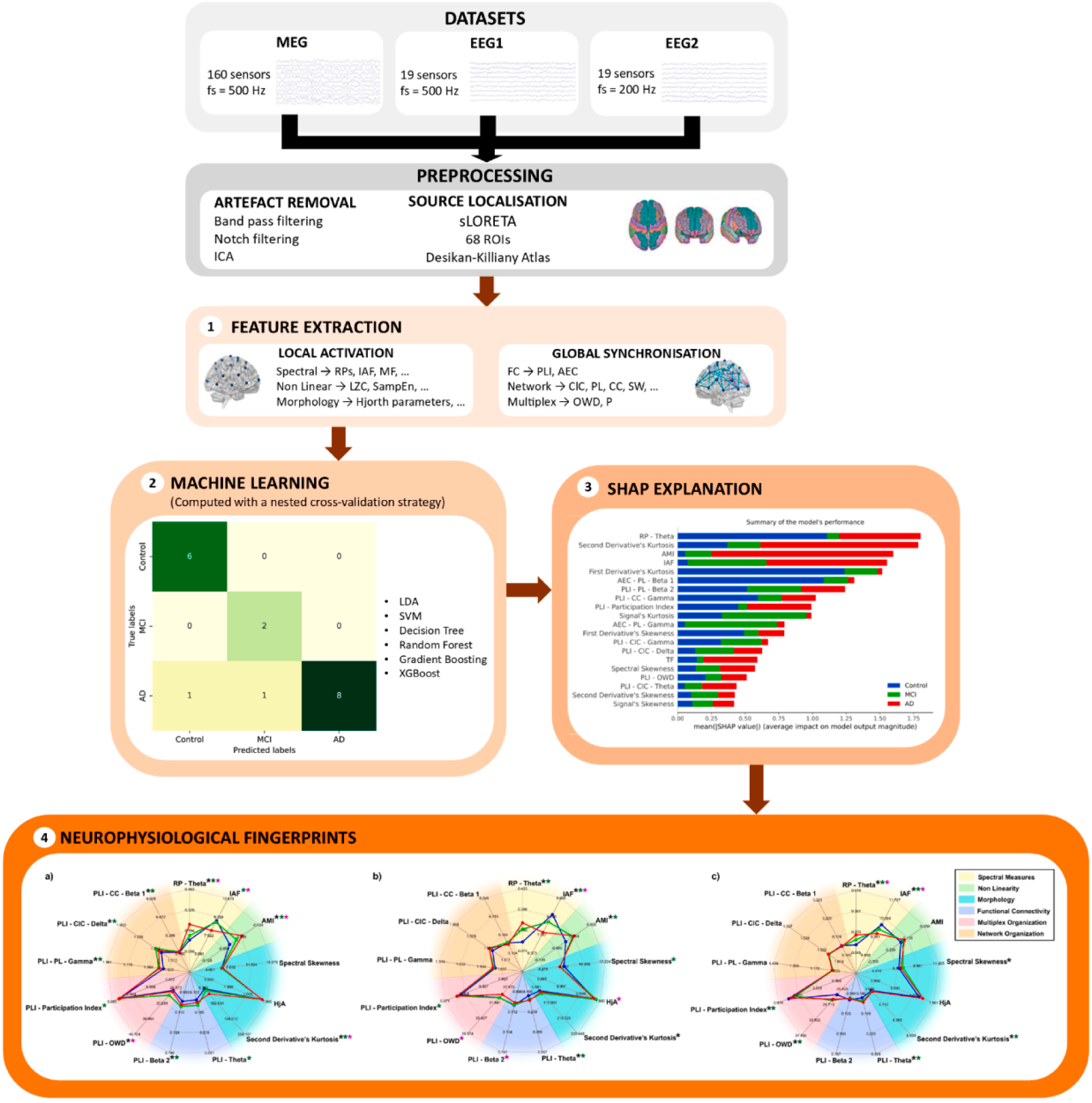

Fig. 1. Flow diagram summarising the methodology to compute the global neurophysiological fingerprints of AD and MCI. As a prior step, the three databases were preprocessed and their source-level time signals were reconstructed: **(1) Feature extraction -** For all subjects, different parameters from local activation and global synchronisation levels were computed to characterise AD and MCI groups; **(2) ML performance -** For each database, different ML classification models were tested by means of a nested cross-validation strategy; **(3) Relevance assessment using SHAP -** The model with the best averaged accuracy was further analysed using the SHAP algorithm to identify the most relevant features; **(4) Neurophysiological fingerprint representation -** From the most relevant parameters selected on step (3), those common to all 3 databases, or at least shared by two of them, were selected.

b) **Non-linear metrics**. The brain has a non-linear behaviour due to threshold and saturation phenomena involved in neuronal dynamics [5]. As a consequence, linear methods may not be precise enough to fully characterise neuronal alterations. Non-linear techniques offer a complementary framework to address this issue [5]. They provide relevant information of non-linear changes due to AD or MCI, such as a loss of complexity, which can be measured by means of the Lempel-Ziv complexity (LZC), Higuchi's fractal dimension (HFD), and Katz's fractal dimension (KFD) [8,40,41]; a reduction in variability, computed by central tendency measure (CTM) [42]; a disruption of predictability, quantified by means of auto-mutual information (AMI) [43]; and alterations in irregularity patterns, observed with approximate entropy (ApEn), sample entropy (SampEn), and fuzzy entropy (FuzzyEn) [14,44,45].

c) **Morphological features**. M/EEG signals are generated by a highly dynamic system, which is characterised by transient and fast rhythmic neural activity. Those rapid fluctuations can be affected by AD and MCI, inducing alterations in the temporal distribution of M/EEG signals and, consequently, in their morphological properties [9,10]. Hjorth's activity (HjA) and mobility (HjM) are parameters useful to quantify the variability and diversity of the morphological changes, respectively [10]. On the other hand, Hjorth's complexity (HjC) estimates the similarity of the signal to a pure sine wave [10]. In addition, statistical moments (i.e., variance, skewness, and kurtosis) of

the spectrum, the original signal, and its first and second derivatives were computed [9,10].

The global synchronisation level evaluates the statistical dependencies between brain regions [46]. In this case, three main categories can be considered:

a) **Functional connectivity parameters**. AD and MCI have been identified as disconnection syndromes [47]; thereby, the assessment of the associated functional connectivity (FC) alterations between M/EEG signals is of paramount importance. To quantify them, two FC metrics were computed [48]: the phase lag index (PLI) to estimate the phase-based coupling and the amplitude envelope correlation (AEC) to measure the amplitude-based connectivity. These parameters were calculated at the conventional frequency bands (delta: 1–4 Hz; theta: 4–8 Hz; alpha: 8–13 Hz; beta 1: 13–19 Hz; beta 2: 19–30 Hz; and gamma: 30–70 Hz), averaging the connectivity weights afterwards to obtain the global connectivity strength for all conventional frequency bands.
b) **Network properties**. The brain functional network is generated by the connectivity patterns between ROIs. Its organisation and structure can be more thoroughly assessed using metrics derived from graph theory. They are useful to summarise complex properties of the brain network: integration, calculated through the characteristic path length (PL) [49]; segregation, computed using the clustering coefficient (ClC) [49]; and centrality, estimated by the closeness centrality (CC) [50].
c) **Multiplex network organisation**. There is evidence of diverse interactions between neural oscillations in different frequency bands [11]. This phenomenon is also observable in frequency-dependent brain networks, where a multilayer structure can be estimated by examining the functional network within each canonical frequency band [11]. This approach allows the computation of different multiplex network properties to assess the organisation of the brain network across levels, considering both phase- (PLI) and amplitude-based (AEC) coupling metrics. Specifically, in this study two multiplex properties were considered: the role of each ROI as a multiplex hub through the computation of the overlapping weighted degree (OWD); and the homogeneity of the connectivity contribution from one ROI to others among layers by means of the participation coefficient (P) [11].

3.2. Machine learning models

ML algorithms manage to recognise patterns and effectively learn to predict or produce automatic decisions [51]. In this study, we tested LDA, SVM, Decision Tree, Random Forest, Gradient Boosting, and XGBoost to assess their classification performances. LDA uses linear hyperplanes to assign input vectors to labelled classes, assuming diverse Gaussian distributions for class generation [52]. SVM model efficiently searches for separating hyperplanes in high-dimensional feature spaces, maximising the margin between classes [53]. Decision Tree employs flowchart-like structures, with nodes representing logical tests and each leaf presenting the predictions [54,55]; it provides an interpretable model, but is prone to over-fitting [54,55]. In that sense, Random Forest mitigates over-fitting by averaging predictions from multiple decision trees built on bootstrap samples [55]. We also used Gradient Boosting, a boosting algorithm that consecutively fits the model to improve estimation by maximising correlation with the negative gradient of the loss function [56]. Finally, XGBoost is an update of Gradient Boosting which is based on learning the negative gradient from the second derivative of the loss function and introduces regularisation to prevent over-fitting and improve efficiency [57].

3.2.1. Feature selection

Of note, the use of a high number of input parameters compared to the number of subjects might lead to over-fitting. This problem is commonly mentioned as the “curse of dimensionality” [58]. In this study feature selection was performed for all ML models; the method employed was fast correlation-based filter (FCBF) [59]. Based on the symmetrical uncertainty [59], FCBF allows the detection of an optimal subset of relevant and non-redundant features, reducing the high dimensionality and complexity of predictive models [60]. Furthermore, it is a filter-type feature selection algorithm, so it provides results that do not depend on posterior analysis [60]. In order to generate a stable subset of parameters, FCBF was applied to 1000 bootstrap iterations for each database. The average significance, defined as the sum of the number of times the features are selected divided by the total number of input features, was used as threshold. Those parameters that were selected a number of times equal or higher than the average significance constituted the optimal subset for each database. Concretely, 32, 28, and 32 features were selected for MEG, EEG1, and EEG2 databases, respectively signals by means of FCBF (for further information, see Supplementary Material).

3.2.2. Hyper-parameter tuning

In order to tune the employed ML models, a grid-search algorithm was performed with the datasets, utilising a nested cross-validation approach. This algorithm is described as two nested loops of cross-validation. The inner loop allows the selection of the hyper-parameters according to the inner cross-validation error, whereas the outer loop evaluates the generalisability of the model on an independent subset [33]. In both loops, a 10-fold cross-validation was implemented. Additional information on the hyper-parameters found by the grid-search is available in the Supplementary Material.

3.2.3. Machine learning model selection

Once the nested cross-validation was performed, different classification scores were obtained from averaging all the nested cross-validation iterations. From them, the model which obtained the best performance in most of the databases for the multi-class classification was selected to undergo the subsequent steps. Furthermore, in the subsequent stages of the methodology, the hyper-parameters associated with the database which obtained the best multi-class performance were selected.

3.3. Shapley additive explanations

The ability to interpret ML-derived results is of paramount importance across different fields. In the case of medical applications, providing an explanation of the contribution of each input variable in group discrimination is essential for decision making [19]. ML systems can operate in intricate and unpredictable manners in which decisions remain concealed. For this reason, XAI methods have been designed to provide further information on the relevance of the input parameters in the model, facilitating the interpretability of the results [19].

In the present study, we used SHAP in order to explain the classification models. By applying SHAP, we uncover the M/EEG features that significantly influence the final classification outcomes. SHAP is a theoretical approach used to provide an explanation to the outcomes of ML models [18]. It generates an additive feature attribution scheme providing a specific predicted importance score to each characteristic. Summing these scores, named SHAP values, it is possible to explain the final decisions. SHAP values represent the contribution of each feature towards prediction performance; thereby, the higher the SHAP value the higher the contribution [18]. Further description of the SHAP algorithm is included in the Supplementary Material. In this study, TreeExplainer was employed to obtain a visual representation of the parameters that most influence the output. TreeExplainer is utilised to estimate SHAP values for tree models and ensembles of trees, under several possible assumptions about feature dependence [61].

3.4. Identification of the neurophysiological fingerprint

Once the ML model that provides the best classification scores was selected and the SHAP algorithm has been applied, a set of input parameters was selected. This subset presents the most relevant M/EEG parameters for the ML model. The selected parameters have to fulfil two requirements: i) relevancy, as it has to be one of the top-half most relevant parameters; and ii) consistency, as these variables have to be shared at least for two out of the three databases. Once the parameters were selected, the representation of the neurophysiological fingerprints was obtained.

Statistically significant differences between pairs of groups were computed for all selected variables by means of the Mann–Whitney test. The significant threshold was set to $\alpha = 0.05$. The multiple comparison problem was addressed by applying false discovery rate (FDR) correction using the Benjamini and Hochberg procedure [62].

Afterwards, Spearman's correlation was computed to measure the similarity between the fingerprints obtained for each group on each database. This provides a measure of the alignment between the three databases and, therefore, about the robustness of the neurophysiological fingerprints.

4. Results

4.1. Models' performance

The metrics used to evaluate the classification performance of the tested models included accuracy and Cohen's kappa, averaged across each iteration of the nested cross-validation. Table 2 summarises binary and three-class classification values for all ML models employed on each database. In addition, Table S2 (in Supplementary Material) presents sensitivity, specificity, precision, negative predictive value, and F1-score values of ML models for each database. For three-class classification, Gradient Boosting outperformed the remaining ML models in terms of Cohen's kappa for the MEG and EEG2 databases, and in accuracy for EEG2 database. On the other hand, for the EEG1 set, the best classification scores were obtained using XGBoost. Finally, although Random Forest presented the highest classification scores for the MEG database in terms of accuracy, Gradient Boosting score was similar.

As Gradient Boosting obtained the best three-class classification performance, it was selected as the model which best discriminates between HC, patients with MCI, and patients with AD. Thus, Gradient Boosting was the ML model considered in next steps.

4.2. SHAP interpretation

In order to provide an interpretation of the most relevant input features for Gradient Boosting, the SHAP algorithm was applied. Specifically, TreeExplainer was used and the SHAP values from all input variables were obtained. Following the criteria stated in Section 3.4, the most relevant variables common to at least two databases were identified. From them, a subset of the most representative metrics for the subgroups of parameters described in 3.1 were selected; that is, for each subgroup of metrics, those who presented the highest averaged SHAP values were included into the subset. These features were:

- **Spectral**: Relative power (RP) in theta frequency band and individual alpha frequency (IAF).
- **Nonlinearity**: Auto-mutual information (AMI).
- **Morphology**: Spectral skewness, Hjorth's activity (HjA), and second derivative's kurtosis.
- **FC**: Phase lag index (PLI) in theta and beta 2 frequency bands.
- **Network properties**: Path length (PL) in gamma frequency band, clustering coefficient (ClC) in delta frequency band, and closeness centrality (CC) in beta 1 frequency band, all of them derived from PLI.
- **Multiplex network organisation**: Participation coefficient (P) and overlapping weighted degree (OWD) derived from PLI.

The relevance of the selected features for the Gradient Boosting model is depicted as summary plots for MEG, EEG1, and EEG2 databases in Figs. 2a, 3a, and 4a, respectively. It can be observed that, for the MEG database, RP in theta frequency band and second derivative's kurtosis are the two most influential variables. This can also be observed in Fig. 2b, and 2c, where the relationships between these parameters and their associated SHAP values can be observed. These figures indicate that the higher the SHAP values assigned to the subjects, the more relevant is the parameter to classify them within the target class. It can be observed that RP in theta frequency band was relevant to HC and AD classification, whereas second derivative's kurtosis played an important role especially for AD discrimination, and AMI and IAF were relevant to AD and MCI classification.

On the other hand, for the EEG1 database, the two most relevant parameters were PLI and RP in theta frequency band. Specifically, these parameters are relevant to HC and AD classification. For the EEG2 database, the two most relevant features were RP in theta frequency band and P derived from PLI. Concretely, RP in theta is relevant to classify HC and AD, and P derived from PLI presents a key role in identifying HC and MCI. The relevance of these parameters in the discrimination can be observed in Figs. 3b and 3c for EEG1, and 4b, 4c for EEG2.

4.3. Neurophysiological fingerprints

Previously selected input variables were used to generate a representation of the neurophysiological fingerprints of AD and MCI. These fingerprints are depicted in Figs. 5a, 5b, and 5c for MEG, EEG1, and EEG2 databases, respectively. It can be observed that, for all three databases, the tendencies were similar, specially between HC and patients with

Table 2
ML models average accuracy and Cohen's kappa values for each database obtained from a nested cross-validation strategy. For both binary and three-class classification approaches, the highest classification statistics on each database were highlighted.

ML Models	Metric	HC vs. all			AD vs. all			Three-class classification		
		MEG	EEG1	EEG2	MEG	EEG1	EEG2	MEG	EEG1	EEG2
LDA	**Accuracy**	87.60 %	80.64 %	75.08 %	**77.13 %**	**83.62 %**	51.03 %	70.67 %	65.40 %	52.61 %
	Cohen's kappa	–	–	–	–	–	–	0.5328	0.4360	0.2697
SVM	**Accuracy**	83.68 %	73.19 %	**77.68 %**	72.40 %	77.69 %	53.13 %	68.92 %	64.88 %	53.03 %
	Cohen's kappa	–	–	–	–	–	–	0.5016	0.4300	2627
Decision Tree	**Accuracy**	**88.10 %**	75.19 %	70.87 %	70.15 %	61.88 %	**57.74 %**	61.14 %	54.97 %	48.92 %
	Cohen's kappa	–	–	–	–	–	–	0.3667	0.2707	0.2255
Random Forest	**Accuracy**	85.94 %	78.12 %	76.13 %	76.70 %	72.26 %	55.71 %	**72.72 %**	64.38 %	50.53 %
	Cohen's kappa	–	–	–	–	–	–	0.5300	0.3991	0.2205
Gradient Boosting	**Accuracy**	86.49 %	**83.57 %**	77.63 %	73.92 %	76.26 %	53.55 %	72.63 %	67.33 %	**53.76 %**
	Cohen's kappa	–	–	–	–	–	–	**0.5452**	0.4593	**0.2729**
XGBoost	**Accuracy**	86.40 %	80.12 %	76.13 %	76.08 %	74.76 %	55.61 %	71.02 %	**69.33 %**	51.26 %
	Cohen's kappa	–	–	–	–	–	–	0.5147	**0.4879**	0.2428

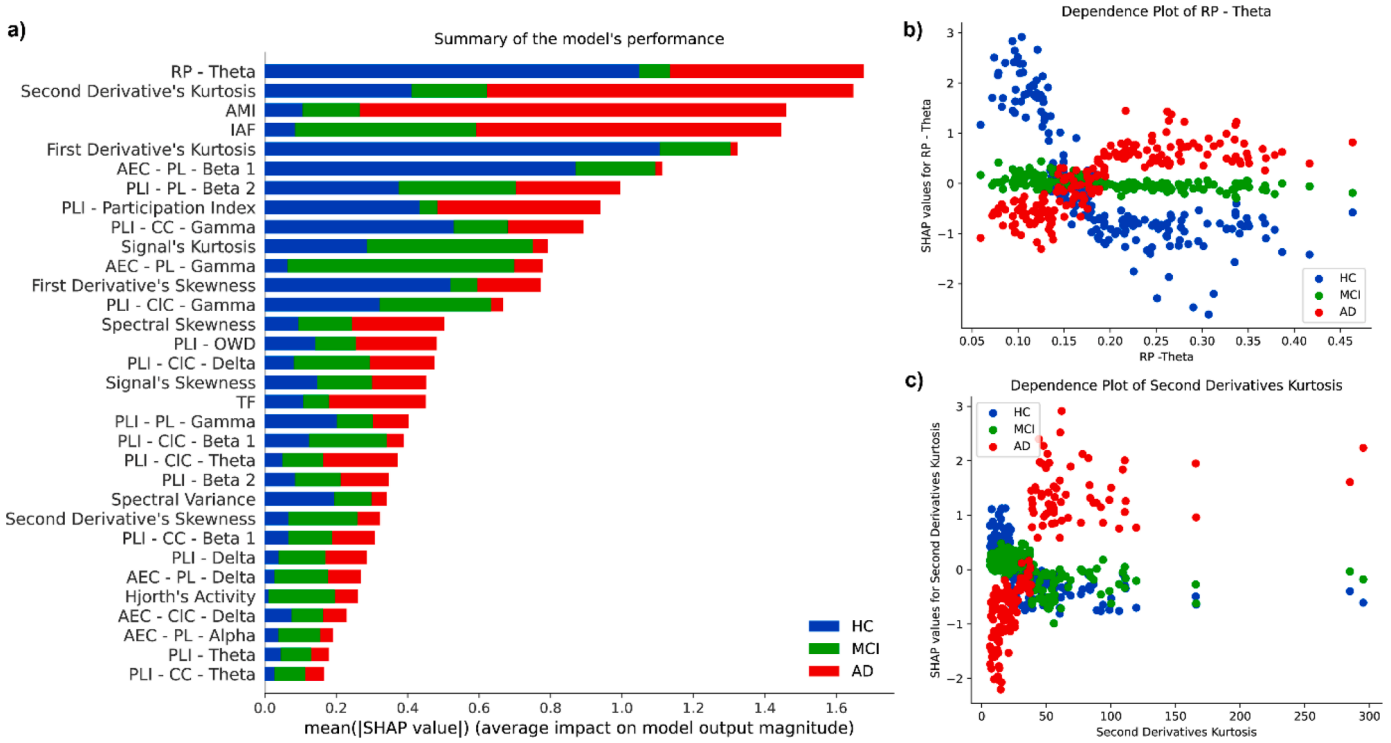

Fig. 2. Influence of the selected input parameters from the MEG database for the Gradient Boosting model measured with SHAP, when classifying the individuals as HC, MCI, or AD: a) Summary plot ranking the variables based on their global influence; b) Dependence plot of RP in theta frequency band, the most influential variable in the MEG database; c) Dependence plot of second derivative's kurtosis, the second most influential variable in the MEG database. Images b) and c) represent the relationship between the parameter values and their corresponding SHAP values; that is, the higher SHAP value associated with the subjects, the more relevance the parameter has to classify them within the target class, and vice versa.

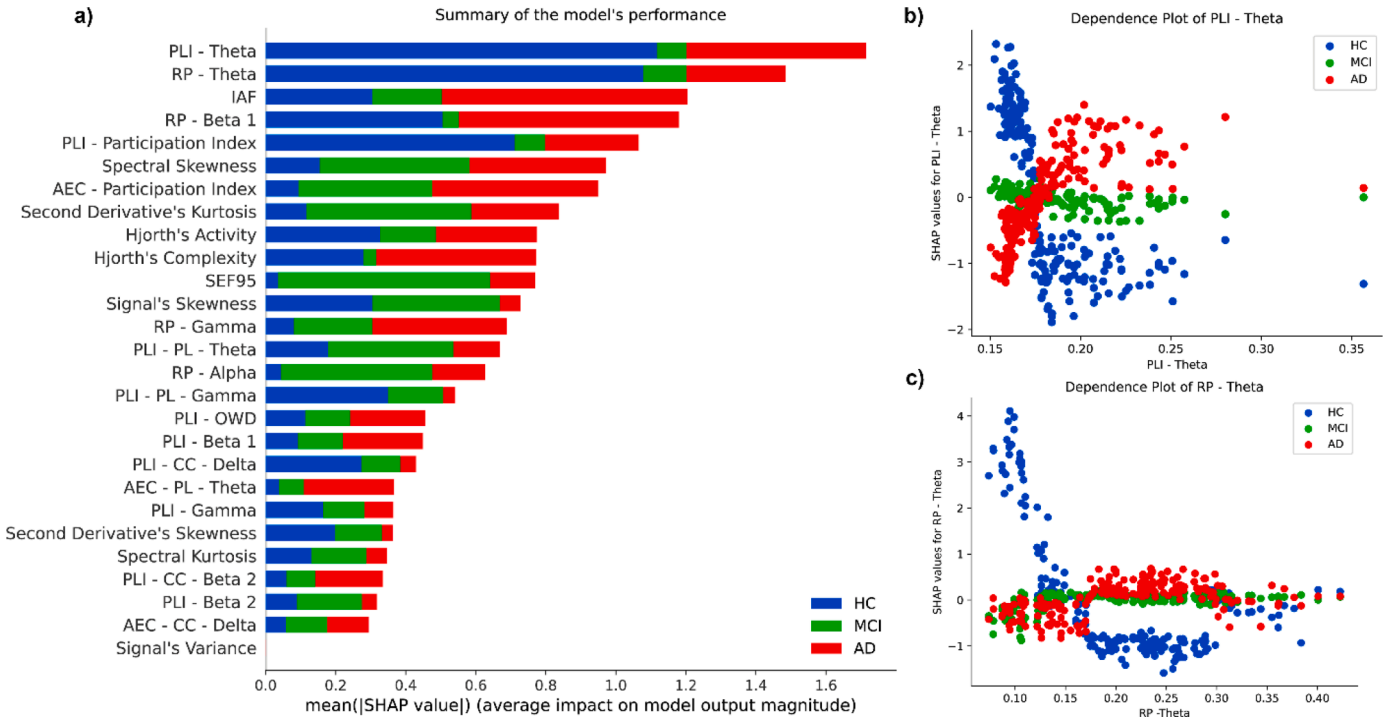

Fig. 3. Influence of the selected input parameters from the EEG1 database for the Gradient Boosting model measured with SHAP, when classifying the individuals as HC, MCI, or AD: a) Summary plot ranking the variables based on their global influence; b) Dependence plot of PLI in theta frequency band, the most influential variable in the EEG1 database; c) Dependence plot of RP in theta frequency band, the second most influential variable in the EEG1 database. Images b) and c) represent the relationship between the parameter values and their corresponding SHAP values; that is, the higher SHAP value associated with the subjects, the more relevance the parameter has to classify them within the target class, and vice versa.

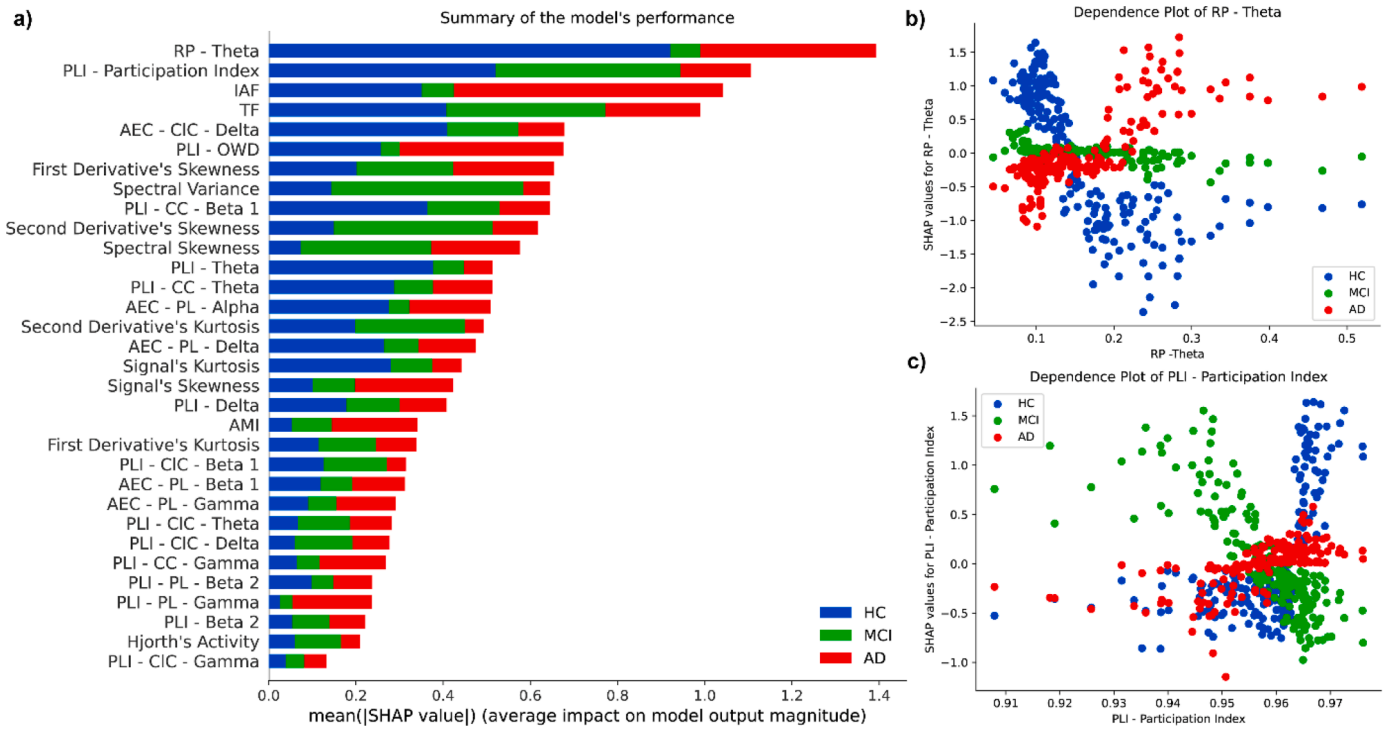

Fig. 4. Influence of the selected input parameters from the EEG2 database for the Gradient Boosting model measured with SHAP, when classifying the individuals as HC, MCI, or AD: a) Summary plot ranking the variables based on their global influence; b) Dependence plot of RP in theta frequency band, the most influential variable in the EEG2 database; c) Dependence plot of P derived from PLI, the second most influential variable in the EEG2 database. Images b) and c) represent the relationship between the parameter values and their corresponding SHAP values; that is, the higher SHAP value associated with the subjects, the more relevance the parameter has to classify them within the target class, and vice versa.

Table 3
Spearman's correlation coefficients between the neurophysiological fingerprints of each database for each group under study (Spearman's rho [*p*-value]).

Groups	Comparisons		
	MEG vs. EEG1	MEG vs. EEG2	EEG1 vs. EEG2
HC	0.9835 ($p < 0.001$)	0.9780 ($p < 0.001$)	0.9615 ($p < 0.001$)
MCI	0.9780 ($p < 0.001$)	0.9505 ($p < 0.001$)	0.9451 ($p < 0.001$)
AD	0.9890 ($p < 0.001$)	0.9615 ($p < 0.001$)	0.9615 ($p < 0.001$)

AD, which supports the replicability of the results across databases. Furthermore, statistically significant differences between pairs of groups were assessed. Shared differences among the three databases were found in spectral, morphology, FC, and multiplex organisation parameters ($p < 0.05$, Mann–Whitney *U*-tests, FDR corrected).

In order to assess the similarity between databases, the Spearman's correlation between the fingerprints obtained for each group on each database was calculated. These values, as well as the associated *p*-values, are included in Table 3. As it can be appreciated, all comparisons showed statistically significant Spearman's correlations, being all of them higher than 0.94 ($p < 0.001$, FDR corrected). These results support the generalisation capability of this methodology.

Moreover, Fig. S1 shows the median values of the parameters given only by the subjects that were successfully classified by the ML model. Even though the tendencies between groups are maintained, the case of the subjects that were correctly classified presents less prominent statistically significant differences between pairs of groups ($p < 0.05$, Mann–Whitney *U*-tests, FDR corrected). Of note, replicability between databases can be also appreciated in Table S3, with statistically significant Spearman's correlation coefficient between the fingerprint obtained for each group on each database ($p < 0.001$, FDR corrected).

5. Discussion

This study aims to characterise the neurophysiological fingerprint of HC, MCI, and AD in order to provide an accurate, interpretable, and robust representation of the disease-induced alterations in the brain electromagnetic activity. To that purpose, different ML-models were applied to analyse their classification performance. Finally, we obtained an interpretation of the three-class classification by assessing the input variables through a XAI approach based on SHAP. Our XAI framework not only provided explanations for the model performance based on the input characteristics, but also allowed us to comprehend how the model interprets the input variables in order to detect whether a subject belongs to a particular group.

5.1. Pursuing an accurate M/EEG-based biomarker

In this study, different ML models were employed to perform binary and multi-class classification between HC, MCI, and AD. Our results showed that, for the HC vs. all classification, Gradient Boosting achieved the highest accuracy values for EEG1 (83.57 %) database, whereas Decision Tree and SVM models achieved the highest accuracy for MEG (88.10 %) and EEG2 (77.68 %) databases, respectively. Additionally, for the AD vs. all discrimination, Decision Tree achieved the highest accuracy for the EEG2 (57.74 %) database, whilst LDA reached the highest accuracy values for MEG (77.13 %) and EEG1 (83.62 %) databases. On the other hand, for multi-class discrimination, Gradient Boosting and XGBoost achieved the highest performance for MEG, EEG1, and EEG2 databases, as observed in Table 2. These accuracy and Cohen's kappa values were 72.63 % and 0.5452 for the MEG database, 69.33 % and 0.4879 for the EEG1 database, and 53.76 % and 0.2729 for the EEG2 database.

There are other studies that performed AD and MCI discrimination (see Table S3) using ML models [14,15,63–75], while others em-

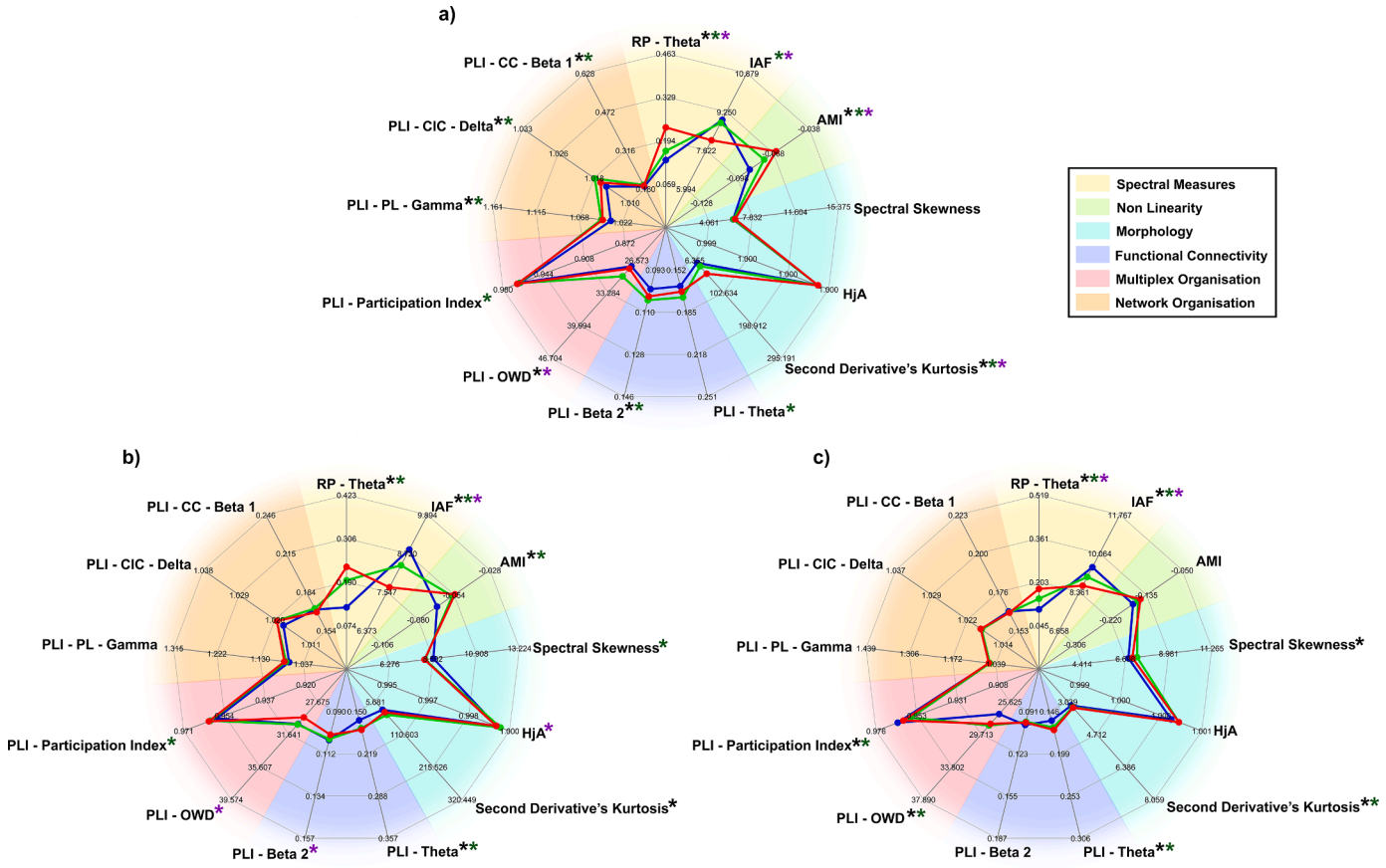

Fig. 5. Median values of the selected variables, representing the neurophysiological fingerprints of AD and MCI. In blue, HC; in green, patients with MCI; in red, patients with AD: a) MEG database; b) EEG1 database; c) EEG2 database. Asterisks represent statistically significant differences between: In black, HC and MCI comparison; in green, HC and AD differences; and in magenta, MCI and AD differentiation ($p < 0.05$, Mann–Whitney U-test, FDR corrected)

ployed ROC curves [40,76–78]. Some of these studies carried out the classification between HC and patients with AD using M/EEG signals, achieving accuracy values that range between 69.00 % and 100 % [15,40,63–70,73–78]. The HC vs. MCI comparison was also addressed in some of these studies, showing accuracy values ranging between 59.48 % and 97.00 % [63,64,66,73,74]. In the case of the discrimination between MCI and AD the accuracies ranged between 49.00 % and 94.05 % [63,64,66,73]. Finally, comparisons between HC vs. all, and AD vs. all were also computed, achieving accuracy values ranging between 76.47 % and 89.00 % [14,73], and between 69.70 % and 74.51 % [14,71]. However, it must be noted that all these studies performed the classification analyses only in one database. Furthermore, most of them employed small databases, which limits their generalisation capability, even though the classification scores are high. Besides, the inclusion of different M/EEG parameters quantifying diverse properties of the brain activity provides detailed information regarding the brain functional organisation. The integration of different brain activity properties provides a more complete and detailed analysis, which might lead to more robust results. Our proposal was designed and assessed in three different databases, including M/EEG recordings, and each one is formed by more than 180 participants. Of note, for the HC vs. all comparison, our models achieved performances close to the maximum values of these ranges, whereas for the AD vs. all discrimination, our results outperformed the previous models. Additionally, for binary classifications, few studies included XAI algorithms in order to assess the relevance of their input parameters [69,70]. However, our approach provides the influence of the most relevant features on each group under study, assessing the influence of those M/EEG parameters on each group.

In the case of multi-class classification between HC, MCI, and AD, other studies obtained accuracy values that range between 58.82 % and 86.00 % [14,72,73], and Cohen's kappa value of 0.2540 [71]. Our multi-class model was assessed in different databases with higher sample sizes, which allowed the analysis of the robustness of our framework. Additionally, in the case of the Cohen's kappa, our methodology outperforms the previous ones in most comparisons. It must be also noted that, for the multi-class discrimination, no studies provided the interpretation on how their input parameters influence their models. The analysis of the relevance of the parameters provides how the model interpreted the input variables to discriminate between HC, MCI, and AD.

5.2. *Towards an interpretable approach for M/EEG-based discrimination model*

The SHAP algorithm provides an interpretation of the influence of input characteristics on the classification statistics [19]. To the best of our knowledge, this is the first study that uses SHAP to evaluate the relevance of different parameters derived from M/EEG recordings in the context of AD and MCI detection.

In the MEG database, RP in theta frequency band and second derivative's kurtosis were the two most relevant parameters for the model's output decision. As it can be observed in Fig. 2a, RP in theta frequency band is relevant for HC and AD classification in opposite manner: in HC, lower RP in theta values are associated with higher SHAP values, and vice-versa in AD group. In addition, second derivative's kurtosis is relevant mainly for AD categorisation, with higher second derivative's kurtosis values related to higher SHAP values. Of note, the opposite

trend is observed for HC and MCI detection. In previous studies, it was found an increase of RP at the theta frequency band in early AD stages, being a typical M/EEG feature of neurodegeneration [79,80]. The second derivative's kurtosis of M/EEG activity quantifies patterns related to rapid increments and decrements of amplitude in the original signal, allowing the analysis of sharp peaks that could remain unnoticed in a visual evaluation [81]. In addition, kurtosis allows the analysis of the data distribution in terms of its peak and tails [9]. The presence of these sharp waves has been detected in epileptiform activity, which has been observed to induce acute effects on cognition and detrimental impairments related to plasticity [82]. In addition, it has been observed that the incidence of beta-amyloid plaques was greater in patients with temporal lobe epilepsy rather than control individuals [82], being a clear biomarker of AD development as well. Therefore, the computation of the kurtosis in the second derivative's M/EEG signal provides further information of the appearance rate of these quick, sharp peaks in the M/EEG activity, allowing a better differentiation between AD patients and HC. On the other hand, the two most relevant parameters for the EEG1 and EEG2 databases were PLI and RP in theta, and RP in theta and P derived from PLI, respectively. Of note, RP in theta was common in all databases, showing its relevance to HC, MCI, and AD discrimination. Additionally, regarding the EEG1 database, increased global PLI values in the theta band have been previously associated with MCI and AD, supporting the hypothesis of the dementia due to AD as a disconnection syndrome [48,83]. In fact, the relationship between theta band connectivity and cognitive decline has been previously assessed, in such a way that the higher the connectivity in theta band, the worse cognitive dysfunction is observed on the patients [84]. For the EEG2 database, P is a metric that evaluates the heterogeneity of the contribution of a node to each of the networks at different frequency bands that make up the multiplex structure [11]. This index quantifies the centrality of different brain regions across frequency bands. Disruption of the multiplex structure, such as in MCI and AD, is suggested to lead to abnormal cognitive and behavioural symptoms [11].

It has been observed that RP in theta presented high relevance to discriminate between subjects in all three databases. Nevertheless, for MEG database, morphology patterns also played a pivotal role in influencing the models, whereas for EEG1 and EEG2 databases FC and multiplex organisation parameters provide higher relevance to the model, respectively.

5.3. Unveiling the neurophysiological fingerprints

The most relevant features of each parameter subgroup were selected to generate the neurophysiological fingerprints of AD and MCI. As observed in Fig. 5, these M/EEG parameters follow similar tendencies in the three databases for both local activation and global synchronisation levels of analysis. Firstly, regarding local activation, it can be observed that RP in theta frequency band and IAF present higher and lower values in AD compared to HC, respectively. In addition, MCI is observed to be an intermediate stage. These patterns were previously shown as markers of the slowing that AD and MCI induce [38,80,85]. In addition, AMI present values closer to zero in AD, compared to HC and MCI. As AMI was observed to be related with entropy, that is, irregularity, values closer to zero are associated with more regular time series [43]. However, differences between HC, MCI, and AD in morphology measures are not as significant as the spectral and non-linear parameters. On the other hand, second derivative's kurtosis was the only morphology parameter that presented statistically significant differences between HC and MCI in all three databases, showing lower values in HC compared to MCI. For the same parameter, differences between HC and AD were found in MEG and EEG2 databases. AD, since its mild stage, could present rapid, sharp peaks compared to the normative state (i.e., HC) [82]. Thus, this measure could be applied as a relevant marker of these signal shapes and provide further information for classification purposes [9,81]. However, spectral skewness and HjA do not present robust statistically significant differences between pairs of groups, as the former presents differences between HC and AD in the EEG1 database, and between HC and MCI in the EEG2 dataset; whereas the latter only displays differences between MCI and AD in the EEG1 database. This may indicate a lower relevance of morphology parameters in order to discriminate HC, MCI, and AD. To sum up, it can be suggested that spectral and non-linear parameters are the most relevant metrics to discriminate pathological and non-pathological states.

Secondly, regarding global synchronisation, the tendencies are not as similar as in the case of local activation. The only parameters that presented consistent statistically significant differences among all three databases were PLI in theta frequency band and P derived from the PLI for the HC and AD comparison. FC parameters, mainly in terms of PLI in theta, show a connectivity increase associated to AD, which is aligned with previous results [48,83]. On the other hand, P derived from PLI presents similar outcomes in MEG and EEG1. In addition, network parameters only exhibit statistically significant differences in the MEG database, although the tendencies are similar in the three databases. As MEG presents a higher number of sensors than the ROIs available in the atlas employed with sLORETA, the definition of the ROIs is more accurate in MEG. This may lead to more precise global synchronisation parameters and, thus, the statistically significant differences that are observed in the network parameters. However, EEG databases present the opposite scenario, which may lead to a less precise definition of the ROIs by means of sLORETA. Due to these opposite scenarios observed in M/EEG databases regarding the significant differences between groups in FC and network organisation features, it can be hypothesised that global synchronisation may play a less relevant role, compared to local activation, to discriminate between HC, MCI, and AD.

Additionally, Spearman's intra-class correlation between databases displayed values higher than 0.94, revealing a clear alignment between databases. The degree of replicability observed in the results derived from M/EEG recordings is of paramount importance to develop a robust approach to address brain disorders analysis, and can contribute to overcome the replication crisis existing in this research field [86]. Therefore, it can be hypothesised that both M/EEG signals, although generated from different neural sources, there is concordance regarding the information that can be extracted from them, which allows their complementary use [87,88]. Furthermore, our results support the idea that AD and MCI exhibit different neurophysiological fingerprints, which diverge from that corresponding to the HC.

5.4. Limitations and future work

While this study has yielded promising results, there are certain limitations that need to be further considered. First, it must be noted that the proposed ML-SHAP framework led to robust results from relatively small databases. The use of deep learning approaches could provide more precise results, although they require larger datasets. Nevertheless, XAI algorithms should be also considered, as deep learning decision-making interpretation must be addressed as well. However, as XAI algorithms relied on local interpretations, the combination of deep learning and XAI in the field of M/EEG should be carefully addressed.

Secondly, it would be interesting to identify differences between correctly classified and misclassified subjects. The analysis of their M/EEG parameters could be useful to improve the discrimination performance. For this task, clustering or community detection algorithms, such as K-means, Newman's or Louvain's algorithm could be useful.

Aligned with the previous ideas, it may be interesting to explore the possibility of training using a database and then, testing the model with another dataset. It may provide a framework to unify databases obtained not only by using different techniques, but also with diverse systems and recorded under different conditions.

Additionally, different M/EEG pre-processing approaches could be assessed to improve the noise reduction. In this regard, it would be interesting to test other pre-processing methods to enhance the generalis-

ability of the outcomes provided not only with M/EEG recordings, but also with different EEG databases.

Next, this approach has been performed by computing M/EEG parameters at source level, in order to find a common ground between MEG and EEG databases. However, it would be interesting to perform the same framework on sensor level signals in future work. That would provide information to check whether a different number of channels would affect the analysis.

Finally, in this work, brain activity has been assessed by means of M/EEG. However, other data such as structural and metabolic information of the brain, socio-demographic and clinical data, and genetics are also relevant for characterising AD and MCI. The model developed in this study could be adapted to analyse different types of data, including those previously mentioned. This might provide a more comprehensive picture of the diseases. In addition, it would be interesting to extend the assessment of the method to other neurological or psychiatric disorders.

6. Conclusions

In this study, we generated the neurophysiological fingerprints of AD and MCI using M/EEG activity through an ML-SHAP framework. For the three-class classification, Gradient Boosting outperformed the other ML models in terms of accuracy and Cohen's kappa for the multi-class classification.

The use of XAI, and particularly the SHAP algorithm, enhanced the interpretability of the ML models. Spectral measures, and specifically RP in theta frequency band, played a relevant role in order to distinguish HC, patients with MCI, and patients with AD in all three databases. However, whilst in the MEG database temporal morphology parameters were also relevant to that purpose, FC and multiplex organisation features presented high relevance in EEG1 and EEG2 datasets, respectively.

The neurophysiological fingerprints generated showed that the three databases presented similar patterns, which support the generalisation ability of the proposed methodology. Our results support the idea that AD and MCI exhibit particular patterns that are different from the normative state, that is, healthy ageing. The neurophysiological fingerprints provide an accurate, interpretable, and robust framework that could help not only for AD and MCI diagnosis, but also for other conditions that affect the central nervous system.

Authorship responsibility

- The material in this manuscript is original.
- The submission has not been previously published or submitted for consideration to another journal.
- I am fully responsible for the content of the manuscript.

CRediT authorship contribution statement

Víctor Gutiérrez-de Pablo: Conceptualization, Methodology, Software, Formal analysis, Investigation, Writing – original draft, Visualization, Data curation; **María Herrero-Tudela:** Conceptualization, Methodology, Formal analysis, Writing – review & editing; **Marina Sandonís-Fernández:** Methodology, Writing – review & editing; **Jesús Poza:** Conceptualization, Methodology, Data curation, Writing – review & editing, Visualization, Supervision, Funding acquisition; **Aarón Maturana-Candelas:** Resources, Data curation, Writing – review & editing; **Víctor Rodríguez-González:** Formal analysis, Writing – review & editing; **Miguel Ángel Tola-Arribas:** Resources, Data curation, Writing – review & editing; **Mónica Cano:** Resources, Data curation, Writing – review & editing; **Hideyuki Hoshi:** Writing – review & editing, Resources, Data curation; **Yoshihito Shigihara:** Writing – review & editing, Resources, Data curation; **Roberto Hornero:** Writing – review & editing, Funding acquisition; **Carlos Gómez:** Conceptualization, Methodology, Data curation, Writing – review & editing, Visualization, Supervision, Funding acquisition.

Declaration of competing interest

None declared.

Acknowledgements

This research was funded by "MICIU/AEI/10.13039/501100011033" and by "ERDF A way of making Europe" through the project PID2022-138286NB-I00 and by "CIBER en Bioingeniería, Biomateriales y Nanomedicina (CIBER-BBN)" through "Instituto de Salud Carlos III" co-funded with ERDF funds. Víctor Gutiérrez-de Pablo and María Herrero-Tudela were in receipt of a PIF-UVa grant from the "University of Valladolid". Marina Sandonís-Fernández was in receipt of a "Ayudas para contratos predoctorales para la Formación de Doctores" grant from the "Ministerio de Ciencia, Innovación y Universidades (CONTFPI-2023-40)".

Supplementary material

Supplementary material associated with this article can be found in the online version at 10.1016/j.bbe.2025.05.011.

References

[1] Gauthier S, Webster C, Servaes S, Morais JA, Rosa-Neto P. World Alzheimer Report 2022—Life after diagnosis: navigating treatment, care and support. Tech. Rep.; Alzheimer's Disease International; London, England; 2022.
[2] Wolk D, Vaishnavi S. Mild cognitive impairment and Alzheimer's disease. In: International neurology. Chichester: John Wiley & Sons, Ltd. ISBN 9781118777329; 2016, p. 133–9. https://doi.org/10.1002/9781118777329.ch39
[3] Jack CR, Bennett DA, Blennow K, Carrillo MC, Dunn B, Haeberlein SB, et al. NIA-AA Research framework: toward a biological definition of Alzheimer's disease. Alzheimer's Dementia 2018;14(4):535–62. https://doi.org/10.1016/j.jalz.2018.02.018
[4] Cassani R, Estarellas M, San-Martin R, Fraga FJ, Falk TH, et al. Systematic review on resting-state EEG for Alzheimer's disease diagnosis and progression assessment. Dis Markers 2018;2018:5174815. https://doi.org/10.1155/2018/5174815
[5] Stam CJ. Nonlinear dynamical analysis of EEG and MEG: review of an emerging field. Clin Neurophysiol 2005;116(10):2266–301. https://doi.org/10.1016/j.clinph.2005.06.011
[6] Babiloni C, Pizzella V, Gratta CD, Ferretti A, Romani GL. Fundamentals of electroencephalography, magnetoencefalography, and functional magnetic resonance imaging. In: International review of neurobiology; vol. 86. Elsevier Inc.; 1st ed., ISBN 9780123748218; 2009, p. 67–80. https://doi.org/10.1016/S0074-7742(09)86005-4
[7] Smailovic U, Jelic V. Neurophysiological markers of Alzheimer's disease: quantitative EEG approach. Neurol Ther 2019;8(s2):37–55. https://doi.org/10.1007/s40120-019-00169-0
[8] Al-Nuaimi A HH, Jammeh E, Sun L, Ifeachor E, et al. Complexity measures for quantifying changes in electroencephalogram in Alzheimer's disease. Complexity 2018;2018:8915079. https://doi.org/10.1155/2018/8915079
[9] Sharma N, Kolekar MH, Jha K, Kumar Y. EEG and cognitive biomarkers based mild cognitive impairment diagnosis. Irbm 2019;40(2):113–21. https://doi.org/10.1016/j.irbm.2018.11.007
[10] Tăuían AM, Casula EP, Pellicciari MC, Borghi I, Maiella M, Bonni S, et al., TMS-EEG perturbation biomarkers for Alzheimer's disease patients classification. Sci Rep 2023;13(1):7667. https://doi.org/10.1038/s41598-022-22978-4
[11] Yu M, Engels M MA, Hillebrand A, Van Straaten E CW, Gouw AA, Teunissen C, et al. Selective impairment of hippocampus and posterior hub areas in Alzheimer's disease: an MEG-based multiplex network study. Brain 2017;140(5):1466–85. https://doi.org/10.1093/brain/awx050
[12] Vecchio DF, Miraglia DF, Iberite DF, Lacidogna DG, Guglielmi DV, Marra DC, et al. Sustainable method for Alzheimer dementia prediction in mild cognitive impairment: electroencephalographic connectivity and graph theory combined with apolipoprotein E. Ann Neurol 2018;84(2):302–14. https://doi.org/10.1002/ana.25289
[13] Gutiérrez-de Pablo V, Poza J, Maturana-Candelas A, Rodríguez-González V, Tola-Arribas MÁ, Cano M, et al. Exploring the disruptions of the neurophysiological organization in Alzheimer's disease: an integrative approach. Comput Methods Programs Biomed 2024;250:108197. https://doi.org/10.1016/j.cmpb.2024.108197
[14] Ruiz-Gómez SJ, Gómez C, Poza J, Gutiérrez-Tobal GC, Tola-Arribas MA, Cano M, et al. Automated multiclass classification of spontaneous EEG activity in Alzheimer's disease and mild cognitive impairment. Entropy 2018;20(1):35. https://doi.org/10.3390/e20010035
[15] Nobukawa S, Yamanishi T, Kasakawa S, Nishimura H, Kikuchi M, Takahashi T, et al. Classification methods based on complexity and synchronization of electroencephalography signals in Alzheimer's disease. Front Psychiatry 2020;11:255. https://doi.org/10.3389/fpsyt.2020.00255

[16] Miltiadous A, Tzimourta KD, Giannakeas N, Tsipouras MG, Afrantou T, Ioannidis P, et al. Alzheimer's disease and frontotemporal dementia: a robust classification method of EEG signals and a comparison of validation methods. Diagnostics 2021;11(8):1437. https://doi.org/10.3390/diagnostics11081437

[17] Barredo Arrieta A, Díaz-Rodríguez N, Del Ser J, Bennetot A, Tabik S, Barbado A, et al. Explainable artificial intelligence (XAI): concepts, taxonomies, opportunities and challenges toward responsible AI. Inf Fusion 2020;58:82–115. https://doi.org/10.1016/j.inffus.2019.12.012

[18] Lundberg SM, Erion G, Chen H, DeGrave A, Prutkin JM, Nair B, et al. From local explanations to global understanding with explainable AI for trees. Nat Mach Intell 2020;2:56–67. https://doi.org/10.1038/s42256-019-0138-9

[19] Band SS, Yarahmadi A, Hsu CC, Biyari M, Sookhak M, Ameri R, et al. Application of explainable artificial intelligence in medical health: a systematic review of interpretability methods. Inform Med Unlocked 2023;40:101286. https://doi.org/10.1016/j.imu.2023.101286

[20] Moral PD, Nowaczyk S, Pashami S. Why is multiclass classification hard? IEEE Access 2022;10(August):80448–62. https://doi.org/10.1109/ACCESS.2022.3192514

[21] McKhann GM, Knopman DS, Chertkow H, Hyman BT, Jack Jr CR, Kawas CH, et al. The diagnosis of dementia due to Alzheimer's disease: recommendations from the national institute on aging- Alzheimer's association workgroups on diagnostic guidelines for Alzheimer's disease. Alzheimer's Dementia 2011;7(3):263–9. https://doi.org/10.1016/j.jalz.2011.03.005

[22] Albert MS, DeKosky ST, Dickson D, Dubois B, Feldman HH, Fox NC, et al. The diagnosis of mild cognitive impairment due to Alzheimer's disease: recommendations from the national institute on aging-Alzheimer's association workgroups on diagnostic guidelines for Alzheimer's disease. Alzheimer's Dementia 2011;7(3):270–9. https://doi.org/10.1176/appi.focus.11.1.96

[23] Rodríguez-González V, Núñez P, Gómez C, Hoshi H, Shigihara Y, Hornero R, et al. Unveiling the alterations in the frequency-dependent connectivity structure of MEG signals in mild cognitive impairment and Alzheimer's disease. Biomed Signal Process Control 2024;87(Part A):105512. https://doi.org/10.1016/j.bspc.2023.105512

[24] Mutanen TP, Metsomaa J, Liljander S, Ilmoniemi RJ, et al. Automatic and robust noise suppression in EEG and MEG: the SOUND algorithm. NeuroImage 2018;166:135–51. https://doi.org/10.1016/j.neuroimage.2017.10.021

[25] Maturana-Candelas A, Gómez C, Poza J, Rodríguez-González V, de Pablo VG, Lopes AM, et al. Influence of PICALM and CLU risk variants on beta EEG activity in Alzheimer's disease patients. Sci Rep 2021;11(1):20465. https://doi.org/10.1038/s41598-021-99589-y

[26] Núñez P, Poza J, Gómez C, Rodríguez-González V, Hillebrand A, Tewarie P, et al. Abnormal meta-state activation of dynamic brain networks across the Alzheimer spectrum. NeuroImage 2021;232:117898. https://doi.org/10.1016/j.neuroimage.2021.117898

[27] Pascual-Marqui RD. Standardized low-resolution brain electromagnetic tomography (sLORETA): technical details. Methods Find Exp Clin Pharmacol 2002;24 Suppl D:5–12.

[28] Tadel F, Baillet S, Mosher JC, Pantazis D, Leahy RM, et al. Brainstorm: a user-friendly application for MEG/EEG analysis. Comput Intell Neurosci 2011;:879716 https://doi.org/10.1155/2011/879716

[29] Desikan RS, Ségonne F, Fischl B, Quinn BT, Dickerson BC, Blacker D, et al. An automated labeling system for subdividing the human cerebral cortex on MRI scans into gyral based regions of interest. NeuroImage 2006;31(3):968–80. https://doi.org/10.1016/j.neuroimage.2006.01.021

[30] Allouch S, Kabbara A, Duprez J, Khalil M, Modolo J, Hassan M, et al. Effect of channel density, inverse solutions and connectivity measures on EEG resting-state networks reconstruction: a simulation study. NeuroImage 2023;271:120006. https://doi.org/10.1016/j.neuroimage.2023.120006

[31] Lin X, Kong W, Li J, Shao X, Jiang C, Yu R, et al. Aberrant static and dynamic functional brain network in depression based on EEG source localization. IEEE/ACM Trans Comput Biol Bioinf 2023;20(3):1876–89. https://doi.org/10.1109/TCBB.2022.3222592

[32] Zhou P, Wu Q, Zhan L, Guo Z, Wang C, Wang S, et al. Alpha peak activity in resting-state EEG is associated with depressive score. Front Neurosci 2023;17:1057908. https://doi.org/10.3389/fnins.2023.1057908

[33] Lemm S, Blankertz B, Dickhaus T, Müller KR. Introduction to machine learning for brain imaging. NeuroImage 2011;56(2):387–99. http://dx.doi.org/10.1016/j.neuroimage.2010.11.004. https://doi.org/10.1016/j.neuroimage.2010.11.004

[34] Wong TT. Performance evaluation of classification algorithms by k-fold and leave-one-out cross validation. Pattern Recognit 2015;48(9):2839–46. https://doi.org/10.1016/j.patcog.2015.03.009

[35] Puri D, Nalbalwar S, Nandgaonkar A, Wagh A. EEG-based diagnosis of Alzheimer's disease using kolmogorov complexity. In: Applied information processing systems. advances in intelligent systems and computing. ISBN 9789811620072; 2022, p. 157–65. https://doi.org/10.1007/978-981-16-2008-9_15

[36] Vecchio F, Babiloni C, Lizio R, De Vico Fallani F, Blinowska K, Verrienti G, et al. Resting state cortical EEG rhythms in Alzheimer's disease: toward EEG markers for clinical applications: a review. In: Supplements to clinical neurophysiology; vol. 62. Elsevier B.V. ISBN 9780702053078; 2013, p. 223–36. https://doi.org/10.1016/B978-0-7020-5307-8.00015-6

[37] Poza J, Gómez C, Bachiller A, Hornero R, et al. Spectral and non-Linear analyses of spontaneous magnetoencephalographic activity in Alzheimer's disease. J Healthc Eng 2012;3(2):299–322. https://doi.org/10.1260/2040-2295.3.2.299

[38] Rodríguez-González V, Gómez C, Hoshi H, Shigihara Y, Hornero R, Poza J, et al. Exploring the interactions between neurophysiology and cognitive and behavioral changes induced by a non-pharmacological treatment: a network approach. Front Aging Neurosci 2021;13:696174. https://doi.org/10.3389/fnagi.2021.696174

[39] Poza J, Hornero R, Escudero J, Fernández A, Sánchez CI, et al. Regional analysis of spontaneous MEG rhythms in patients with alzheimer's disease using spectral entropies. Ann Biomed Eng 2008;36(1):141–52. https://doi.org/10.1007/s10439-007-9402-y

[40] Gómez C, Mediavilla Á, Hornero R, Abásolo D, Fernández A, et al. Use of the Higuchi's fractal dimension for the analysis of MEG recordings from Alzheimer's disease patients. Med Eng Phys 2009;31(3):306–13. https://doi.org/10.1016/j.medengphy.2008.06.010

[41] Raghavendra BS, Narayana Dutt D. A note on fractal dimensions of biomedical waveforms. Comput Biol Med 2009;39(11):1006–12. https://doi.org/10.1016/j.compbiomed.2009.08.001

[42] Abásolo D, Hornero R, Gómez C, García M, López M, et al. Analysis of EEG background activity in Alzheimer's disease patients with Lempel–Ziv complexity and central tendency measure. Med Eng Phys 2006;28(4):315–22. https://doi.org/10.1016/j.medengphy.2005.07.004

[43] Gómez C, Hornero R, Abásolo D, Fernández A, Escudero J. Analysis of the magnetoencephalogram background activity in Alzheimer's disease patients with auto-mutual information. Comput Methods Programs Biomed 2007;87(3):239–47. https://doi.org/10.1016/j.cmpb.2007.07.001

[44] Espinosa R, Talero J, Weinstein A. Effects of tau and sampling frequency on the regularity analysis of ECG and EEG signals using apen and sampen entropy estimators. Entropy 2020;22(11):1298. https://doi.org/10.3390/e22111298

[45] Monge J, Gómez C, Poza J, Fernández A, Quintero J, Hornero R, et al. MEG analysis of neural dynamics in attention-deficit/hyperactivity disorder with fuzzy entropy. Med Eng Phys 2015;37(4):416–23. https://doi.org/10.1016/j.medengphy.2015.02.006

[46] O'Neill GC, Tewarie P, Vidaurre D, Liuzzi L, Woolrich MW, Brookes MJ, et al. Dynamics of large-scale electrophysiological networks: a technical review. NeuroImage 2018;180:559–76. https://doi.org/10.1016/j.neuroimage.2017.10.003

[47] Stam CJ, van Straaten E CW. The organization of physiological brain networks. Clin Neurophysiol 2012;123(6):1067–87. https://doi.org/10.1016/j.clinph.2012.01.011

[48] Briels CT, Schoonhoven DN, Stam CJ, De Waal H, Scheltens P, Gouw AA, et al. Reproducibility of EEG functional connectivity in Alzheimer's disease. Alzheimer's Res Ther 2020;12(1):68. https://doi.org/10.1186/s13195-020-00632-3

[49] Stam CJ, De Haan W, Daffertshofer A, Jones BF, Manshanden I, Van Cappellen Van Walsum AM, et al., et al. Graph theoretical analysis of magnetoencephalographic functional connectivity in Alzheimer's disease. Brain 2009;132(1):213–24. https://doi.org/10.1093/brain/awn262

[50] Rubinov M, Sporns O. Complex network measures of brain connectivity: uses and interpretations. NeuroImage 2010;52(3):1059–69. https://doi.org/10.1016/j.neuroimage.2009.10.003

[51] Krueger C, Bini S, Helm JM, Swiergosz AM, Haeberle HS, Karnuta JM, et al. Machine learning and artificial intelligence: definitions, applications, and future directions. Curr Rev Musculoskelet Med 2020;13(1):69–76. https://doi.org/10.1007/s12178-020-09600-8

[52] Bishop CM, et al. Pattern recognition and machine learning. Springer New York, NY; 1st ed., 2006. ISBN 9780387310732. https://doi.org/10.1007/978-3-030-57077-4_11

[53] Mammone A, Turchi M, Cristianini N. Support vector machines. Wiley Interdiscip Rev 2009;1(3):283–9. https://doi.org/10.1002/wics.49

[54] Costa VG, Pedreira CE. Recent advances in decision trees: an updated survey. Artif Intell Rev 2023;56:4765–800. https://doi.org/10.1007/s10462-022-10275-5

[55] Schonlau M, Zou RY. The random forest algorithm for statistical learning. Stata J 2020;20(1):3–29. https://doi.org/10.1177/1536867X20909688

[56] Natekin A, Knoll A. Gradient boosting machines, a tutorial. Front Neurorobot 2013;7:21. https://doi.org/10.3389/fnbot.2013.00021

[57] Chen T, Guestrin C. XGBoost: a scalable tree boosting system. In: Proceedings of the ACM SIGKDD international conference on knowledge discovery and data mining. ISBN 9781450342322; 2016, p. 785–94. https://doi.org/10.1145/2939672.2939785

[58] Berisha V, Krantsevich C, Hahn PR, Hahn S, Dasarathy G, Turaga P, et al. Digital medicine and the curse of dimensionality. npj Digit Med 2021;4(1):153. https://doi.org/10.1038/s41746-021-00521-5

[59] Yu L, Liu H. Efficient feature selection via analysis of relevance and redundancy. J Mach Learn Res 2004;5:1205–24.

[60] Guyon I, Elisseeff A. An introduction to variable and feature selection. J Mach Learn Res 2003;3:1157–82.

[61] shap.TreeExplainer - SHAP latest documentation. 2025 https://shap-lrjball.readthedocs.io/en/latest/generated/shap.TreeExplainer.html.

[62] Benjamini Y, Hochberg Y. Controlling the false discovery rate: a practical and powerful approach to multiple testing. J R Stat Soc Ser B (Methodological) 1995;57(1):289–300. doi:0035-9246/95/57289

[63] Bruña R, Poza J, Gómez C, García M, Fernández A, Hornero R, et al. Analysis of spontaneous MEG activity in mild cognitive impairment and Alzheimer's disease using spectral entropies and statistical complexity measures. J Neural Eng 2012;9(3). https://doi.org/10.1088/1741-2560/9/3/036007

[64] Buscema M, Vernieri F, Massini G, Scrascia F, Breda M, Rossini PM, et al. An improved I-FAST system for the diagnosis of Alzheimer's disease from unprocessed electroencephalograms by using robust invariant features. Artif Intell Med 2015;64(1):59–74. https://doi.org/10.1016/j.artmed.2015.03.003

[65] Chedid N, Tabbal J, Kabbara A, Allouch S, Hassan M. The development of an automated machine learning pipeline for the detection of Alzheimer's disease. Sci Rep 2022;12(1):6–12. https://doi.org/10.1038/s41598-022-22979-3
[66] Ding Y, Chu Y, Liu M, Ling Z, Wang S, Li X, et al. Fully automated discrimination of Alzheimer's disease using resting-state electroencephalography signals. Quant Imaging Med Surg 2022;12(2):1063–78. https://doi.org/10.21037/qims-21-430
[67] Furutani N, Nariya Y, Takahashi T, Noto S, Yang AC, Hirosawa T, et al. Decomposed temporal complexity analysis of neural oscillations and machine learning applied to Alzheimer's disease diagnosis. Front Psychiatry 2020;11:531801. https://doi.org/10.3389/fpsyt.2020.531801
[68] Hornero R, Escudero J, Fernández A, Poza J, Gómez C, et al. Spectral and nonlinear analyses of MEG background activity in patients with Alzheimer's disease. IEEE Trans Biomed Eng 2008;55(6):1658–65. https://doi.org/10.1109/TBME.2008.919872
[69] Khare SK, Acharya UR. Adazd-Net: automated adaptive and explainable Alzheimer's disease detection system using EEG signals. Knowledge-Based Syst 2023;278:110858. https://doi.org/10.1016/j.knosys.2023.110858
[70] Lal U, Chikkankod AV, Longo L. A comparative study on feature extraction techniques for the discrimination of frontotemporal dementia and Alzheimer's disease with electroencephalography in resting-state adults. Brain Sci 2024;14(4):335. https://doi.org/10.3390/brainsci14040335
[71] Maturana-Candelas A, Gómez C, Poza J, Pinto N, Hornero R, et al. EEG characterization of the Alzheimer's disease continuum by means of multiscale entropies. Entropy 2019;21(6):544. https://doi.org/10.3390/e21060544
[72] McBride JC, Zhao X, Munro NB, Smith CD, Jicha GA, Hively L, et al. Spectral and complexity analysis of scalp EEG characteristics for mild cognitive impairment and early Alzheimer's disease. Comput Methods Programs Biomed 2014;114(2):153–63. https://doi.org/10.1016/j.cmpb.2014.01.019
[73] Pirrone D, Weitschek E, Di Paolo P, De Salvo S, De Cola MC. EEG Signal processing and supervised machine learning to early diagnose Alzheimer's disease. Appl Sci 2022;12(11):5413. https://doi.org/10.3390/app12115413
[74] Poza J, Gómez C, García M, Tola-Arribas MA, Carreres A, Cano M, et al. Spatio-temporal fluctuations of neural dynamics in mild cognitive impairment and Alzheimer's disease. Curr Alzheimer Res 2017;14(9):924–36. https://doi.org/10.2174/1567205014666170309115656
[75] Trambaiolli LR, Spolaôr N, Lorena AC, Anghinah R, Sato JR. Feature selection before EEG classification supports the diagnosis of Alzheimer's disease. Clin Neurophysiol 2017;128(10):2058–67. https://doi.org/10.1016/j.clinph.2017.06.251
[76] Abásolo D, Escudero J, Hornero R, Gómez C, Espino P. Approximate entropy and auto mutual information analysis of the electroencephalogram in Alzheimer's disease patients. Med Biol Eng Comput 2008;46(10):1019–28. https://doi.org/10.1007/s11517-008-0392-1
[77] Gómez C, Hornero R, Abásolo D, Fernández A, López M, et al. Complexity analysis of the magnetoencephalogram background activity in Alzheimer's disease patients. Med Eng Phys 2006;28(9):851–9. https://doi.org/10.1016/j.medengphy.2006.01.003
[78] Poza J, Hornero R, Abásolo D, Fernández A, García M. Extraction of spectral based measures from MEG background oscillations in Alzheimer's disease. Med Eng Phys 2007;29(10):1073–83. https://doi.org/10.1016/j.medengphy.2006.11.006
[79] Dauwels J, Srinivasan K, Ramasubba Reddy M, Musha T, Vialatte F-B, Latchoumane C, et al. Slowing and loss of complexity in Alzheimer's EEG: two sides of the same coin? Int J Alzheimers Dis 2011;2011:539621. https://doi.org/10.4061/2011/539621
[80] Bhattacharya BS, Coyle D, Maguire LP. Alpha and theta rhythm abnormality in Alzheimer's disease: a study using a computational model. Adv Exp Med Biol 2011;718:57–73. https://doi.org/10.1007/978-1-4614-0164-3_6
[81] Birkemeier WP, Fontaine AB, Celesia GG, Ma KM. Pattern recognition techniques for the detection of epileptic transients in EEG. IEEE Trans Biomed Eng 1978;25(3):213–17. https://doi.org/10.1109/TBME.1978.326324
[82] Vossel KA, Tartaglia MC, Nygaard HB, Zeman AZ, Miller BL. Epileptic activity in Alzheimer's disease: causes and clinical relevance. Lancet Neurol 2017;16(4):311–22. http://dx.doi.org/10.1016/S1474-4422(17)30044-3. https://doi.org/10.1016/S1474-4422(17)30044-3
[83] Schoonhoven DN, Briels CT, Hillebrand A, Scheltens P, Stam CJ, Gouw AA, et al. Sensitive and reproducible MEG resting-state metrics of functional connectivity in Alzheimer's disease. Alzheimer's Res Ther 2022;14(1):38. https://doi.org/10.1186/s13195-022-00970-4
[84] Canuet L, Tellado I, Couceiro V, Fraile C, Fernandez-Novoa L, Ishii R, et al. Resting-state network disruption and APOE genotype in Alzheimer's disease: a lagged functional connectivity study. PLoS One 2012;7(9):1–12. https://doi.org/10.1371/journal.pone.0046289
[85] Okumura E, Hoshi H, Morise H, Okumura N, Fukasawa K, Asakawa T, et al. Reliability of spectral features of resting-state brain activity: a magnetoencephalography study. Cureus 2024;16(1):e52637. https://doi.org/10.7759/cureus.52637
[86] Niso G, Krol LR, Combrisson E, Dubarry AS, Elliott MA, François C, et al. Good scientific practice in EEG and MEG research: progress and perspectives. NeuroImage 2022;257:119056. https://doi.org/10.1016/j.neuroimage.2022.119056
[87] Rampp S, Stefan H. On the opposition of EEG and MEG. Clin Neurophysiol 2007;118(8):1658–9. https://doi.org/10.1016/j.clinph.2007.04.021
[88] Olsen AS, Høegh R MT, Hinrich JL, Madsen KH, Mørup M. Combining electro- and magnetoencephalography data using directional archetypal analysis. Front Neurosci 2022;16:911034. https://doi.org/10.3389/fnins.2022.911034